ADVANCED HEALTHCARE MATERIALS
www.advhealthmat.de

Tuning Embryoid Germ Layer Specification in Tryptophan Zipper Hydrogels Through Pendant Matrix-Derived Motifs

*Ashley K. Nguyen, Md Shariful Islam, Riddhesh B. Doshi, Mengbai Yu, Sara Romanazzo, Juanfang Ruan, Richard D. Tilley, Tushar Kumeria, Jitendra Mata, and Kristopher A. Kilian**

The ability of stem cells to sense and respond to nanoscale features in their microenvironment underscores the need for tunable hydrogel nanostructures in matrices for biofabrication. Here, a modular hydrogel platform is presented that uses tryptophan zipper (Trpzip) based peptides functionalized with extracellular matrix-derived adhesive motifs to create shear thinning bioactive synthetic hydrogels with tunable mechanical and biochemical properties. Rheological and small-angle neutron scattering analyses reveal that while the addition of GRGDS, GFOGER, YIGSR, or IKVAV motifs has minimal impact on nanofiber diameter and bulk hydrogel stiffness, they significantly alter nanofiber flexibility and microscale hierarchical organization of Trpzip networks. In concert with adhesive cues, these subtle differences in overall hydrogel architecture influence lineage commitment of 3D encapsulated human induced pluripotent stem cell embryoids. Trpzip matrices presenting GRGDS best support mesodermal fates, IKVAV promotes ectodermal commitment, and unmodified Trpzip matrices with no adhesive cues enhance endodermal differentiation. The results suggest that ligand-driven modulation of nanofiber rigidity and entanglement can contribute to pluripotent stem cell lineage specification, supporting the potential of Trpzip hydrogels as customizable reagents for biofabrication, stem cell manufacture, tissue engineering, and regenerative medicine.

1. Introduction

In native tissues, cells inhabit highly organized fibrillar microenvironments defined by controlled spatial organization of extracellular matrix (ECM) proteins. This complex biochemical and mechanical landscape is essential for regulating tissue development and directing stem cell fate. For human induced pluripotent stem cells (iPSCs), these matrix-derived cues are essential for maintaining self-renewal properties[1] or driving commitment into specific tissue lineages.[2] However, conventional iPSC culture systems, typically based on 2D polystyrene or glass substrates, fail to emulate the 3D, spatially-controlled architecture of the in vivo niche. Furthermore, most iPSC differentiation protocols rely on Matrigel, a complex and poorly defined animal-derived ECM mixture that presents a wide array of adhesion ligands simultaneously,[3–6] making it difficult to disentangle the specific effects of individual matrix signals.

To overcome these limitations, there is growing interest in engineering synthetic stem cell niches that present user-defined biochemical cues in a controlled mechanical microenvironment. Among synthetic hydrogel platforms, peptide-based systems offer unique advantages owing to their well-defined chemical composition, inherent cytocompatibility,[7] and ability to form nanofibrillar structures reminiscent of native ECM proteins.[8] However, the incorporation of adhesive motifs to achieve

A. K. Nguyen, R. B. Doshi, S. Romanazzo, R. D. Tilley, J. Mata, K. A. Kilian
School of Chemistry
University of New South Wales
Sydney, NSW 2052, Australia
E-mail: k.kilian@unsw.edu.au
M. S. Islam, M. Yu, T. Kumeria, K. A. Kilian
School of Materials Science and Engineering
University of New South Wales
Sydney, NSW 2052, Australia
J. Ruan, R. D. Tilley
Electron Microscopy Unit
Mark Wainwright Analytical Centre
University of New South Wales
Sydney, NSW 2052, Australia
R. D. Tilley, T. Kumeria, K. A. Kilian
Australian Centre for Nanomedicine
University of New South Wales
Sydney, NSW 2052, Australia
J. Mata
Australian Centre for Neutron Scattering
Australian Nuclear Science and Technology Organization
Lucas Heights, NSW 2234, Australia
K. A. Kilian
School of Clinical Medicine
Faculty of Medicine and Health
University of New South Wales
Sydney, NSW 2052, Australia

The ORCID identification number(s) for the author(s) of this article can be found under https://doi.org/10.1002/adhm.202503600

DOI: 10.1002/adhm.202503600

sufficient cellular recognition while maintaining network architecture and the desired mechanical properties remains a central biomaterial design challenge. Many peptide hydrogels require chemical modification,[9–12] co-polymerization with xenogenic ECM proteins,[13] or suffer from limited control over supramolecular organization, all of which can compromise reproducibility and translation applicability.

We previously introduced a short self-assembling peptide known as the tryptophan zipper (Trpzip), which forms nanofibrous hydrogels under physiological conditions, with unique yield-stress properties that support suspension bioprinting, and innate bioactivity without the need for canonical adhesion ligands.[14] In the current study, we expand on this platform by incorporating a series of ECM-derived adhesive ligands including GRGDS (fibronectin),[15] GFOGER (collagen I),[16] YIGSR (laminin β1),[17] and IKVAV (laminin α1)[18] into the original Trpzip backbone. We systematically evaluate how these adhesive cues influence both the nanoscale assembly and the cellular bioactivity of Trpzip hydrogels. Using small-angle neutron scattering (SANS) and rheological measurements, we characterized changes in nanofiber rigidity, network structure, and mechanical behavior upon ligand incorporation. In addition, we investigated the ability of Trpzip-ligand hydrogels to support iPSC viability, pluripotency, and directed trilineage germ layer differentiations in 3D culture. Notably, we observe that specific ligands promote distinct lineage specification, suggesting that the interplay between matrix mechanics, nanofiber architecture, and adhesive presentation together shape the differentiation fate of encapsulated iPSCs. This modular approach allows for fine tuning of the tissue–hydrogel interface while preserving the desirable nanostructure and mechanical properties of Trpzip matrices.

2. Results and Discussion

We previously reported that tryptophan zipper (Trpzip) based short peptides can self-assemble into nanofibrous hydrogels under physiological conditions and support the growth and proliferation of mammalian cells and organoids encapsulated within, without the need for canonical cell-adhesive ligands such as RGD.[14] However, in some circumstances, additional bioactive cues could prove advantageous for directing cell activity. To explore whether the incorporation of ECM-derived cell-adhesion ligands into Trpzip matrices could further modulate cell behavior, we created a series of Trpzip-ligand peptides derived from common ECM proteins by appending GRGDS (Fibronectin), GFOGER (Collagen), YIGSR, or IKVAV (Laminin) to the C-terminus of the self-assembling Trpzip core motif (**Figure 1A**). Here, we utilized the optimized Trpzip peptide with a glutamate and valine substitution in the fifth and eighth positions in the sequence, as described in previous work.[14] All binding motifs were added to the Trpzip sequence without the use of any flexibility linkers. These ligand-bearing Trpzip peptides were then mixed with unmodified Trpzip to generate functionalized matrices for 3D stem cell culture, where the adhesion sequence is diluted within the matrix to provide adequate space for integrin-mediated biorecognition. Trpzip-ligand peptides were dissolved in water and mixed with a 1% (w/v) solution of free Trpzip peptides to achieve a concentration of 200 μM of ligand in the final hydrogel. The resulting Trpzip solution was then mixed in a 1:1 volumetric ratio with DMEM to trigger gelation via ionic screening, producing hydrogels comprised of 5 mg mL^{-1} free Trpzip peptide with an additional 200 μM Trpzip-ligand peptide. All Trpzip-ligand formulations gelled rapidly under these conditions, with visual and qualitative behavior very similar to that of unmodified Trpzip hydrogels.

To assess whether the incorporation of adhesive motifs altered hydrogel mechanics, we performed oscillatory shear rheology. Time sweep measurements revealed that all formulations exhibited similar gelation kinetics, with the storage moduli plateau reached within ≈5 h (Figure 1B). While Trpzip-GRGDS and Trpzip-GFOGER hydrogels achieved stiffnesses of 777 ± 193 and 722 ± 136 Pa, respectively, Trpzip-YIGSR and Trpzip-IKVAV hydrogels reached higher G' values of 1323 ± 191 and 1119 ± 394 Pa (Figure 1C), possibly reflecting enhanced cross-linking or favorable packing interactions conferred by the ligand sequences, although further characterization is needed to ascertain this. Notably, hydrogels composed entirely of Trpzip-ligand peptides could also be formed (Figure S1, Supporting Information). For instance, although gels formed from 100% Trpzip-GRGDS showed comparable mechanical stability to unmodified Trpzip hydrogels, they exhibited slower gelation as defined by their t_{90} value (time taken to reach 90% of final stiffness), which was 10.1 h compared to 8.4 h for Trpzip only. They also exhibited a lower overall stiffness (351 ± 13 Pa compared to 812 ± 179 Pa for Trpzip only), likely due to disruption of the Trpzip self-assembly pathway, ultimately limiting their suitability for in vitro applications.

Strain sweeps were also performed to probe the mechanical stability of each Trpzip-ligand hydrogel (Figure 1D). All formulations exhibited a characteristic yield point, defined here as the strain at which G' decreases by 10% from its plateau value in the linear viscoelastic region. Unmodified Trpzip hydrogels yielded at 0.29% strain, consistent with previous findings,[14] while Trpzip-GRGDS, Trpzip-GFOGER, and Trpzip-YIGSR hydrogels yielded at lower strains of 0.17%, 0.21%, and 0.23%, respectively, indicating slightly decreased network stability (Figure 1E). Trpzip-IKVAV hydrogels displayed the highest yield point at 0.47%, suggesting that incorporation of the IKVAV motif improves not only the initial cross-linking of the Trpzip network, but also provides additional mechanical stability post-gelation.

Altogether, these results demonstrate that Trpzip peptides can be functionally modified with a range of cell-adhesive ligands without substantially altering their ability to form robust hydrogels. This modular design provides a tunable platform for creating biomimetic microenvironments with both defined mechanical and biochemical cues, supporting their use as synthetic niches for guiding iPSC differentiation.

Next, to investigate how Trpzip-ligand incorporation affects the nanostructure and hierarchical organization of the resultant hydrogels, we performed small-angle neutron scattering (SANS) on a variety of liquid and gelled Trpzip formulations. We previously reported that Trpzip peptides assemble into stacked disc-like lamellae, which organize into nanofibers that subsequently entangle into branched microscale aggregates in buffered solutions.[14] To better characterize the initial stages of Trpzip self-assembly, scattering profiles were acquired for Trpzip peptides dissolved in deuterated water (D_2O), representing the pre-gelation state, across a concentration series (**Figure 2A**).

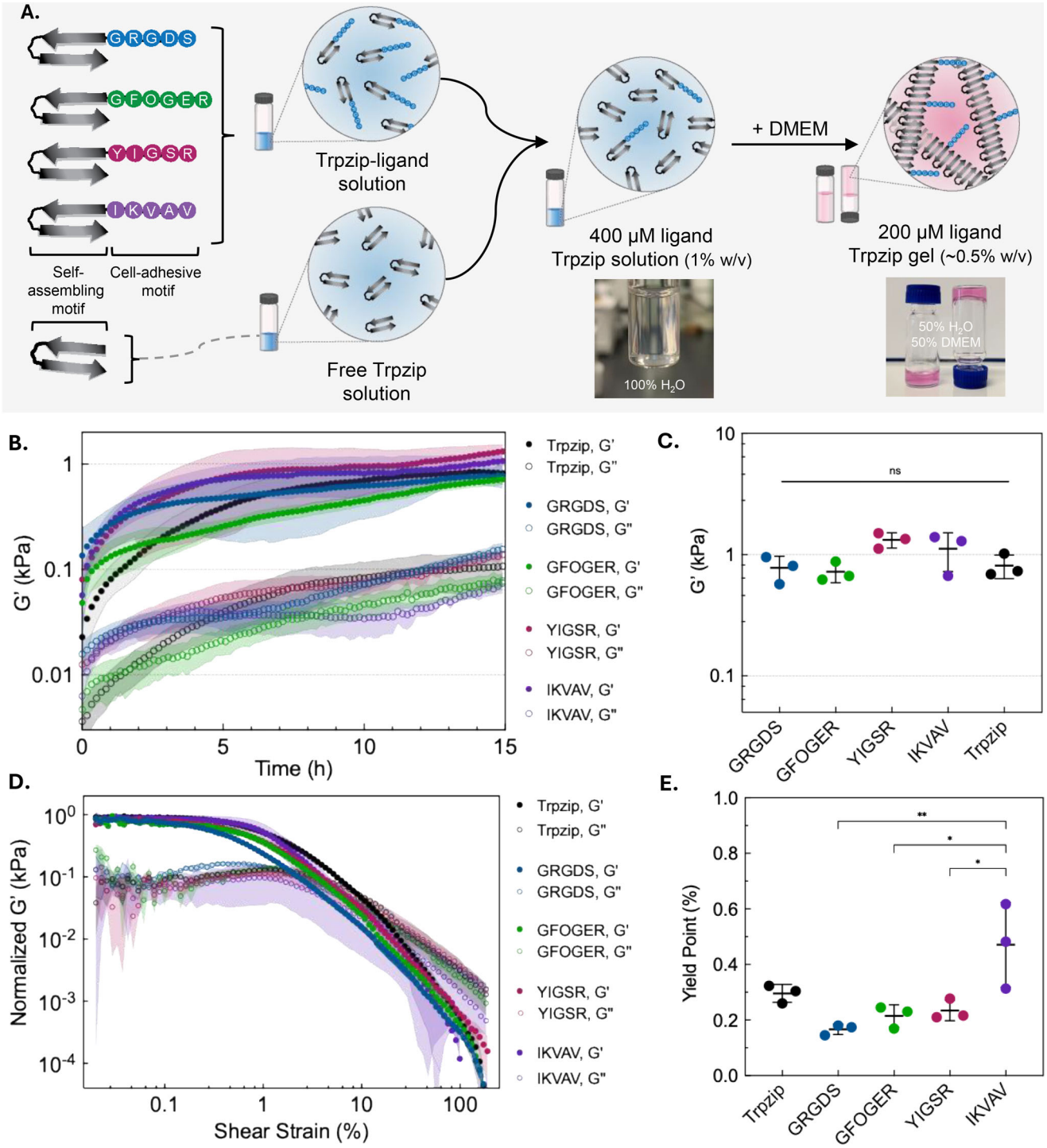

Figure 1. Trpzip hydrogel preparation strategy and mechanical characterization of various Trpzip hydrogel formulations. A) Schematic of the hydrogel formulation process for ligand-functionalized Trpzip hydrogels. Trpzip-based peptides bearing different cell-adhesive motifs (GRGDS, GFOGER, YIGSR, IKVAV) were synthesized by appending each motif to the C-terminus of a self-assembling Trpzip domain. These Trpzip-ligand peptides were dissolved in water and added to a solution of free Trpzip peptides at 200 μ, then mixed 1:1 with cell culture media (e.g., DMEM or mTeSR) to induce self-assembly and hydrogel formation. B) Time sweep rheology showing the evolution of storage modulus (G′, closed symbols) and loss modulus (G″, open symbols) over 15 h of gelation for each Trpzip-ligand hydrogel. C) Equilibrium stiffnesses for Trpzip and Trpzip-ligand hydrogels. Data is shown as mean ± s.d. from n = 3 independently prepared gels. Statistical significance was determined using a one-way ANOVA with Tukey's post-hoc test ($p < 0.05$ considered significant). D) Strain sweep rheology showing the nonlinear mechanical response for each Trpzip-ligand hydrogel. E) Yield points for Trpzip and Trpzip-ligand hydrogels. Data is shown as mean ± s.d. from n = 3 independently prepared gels. Statistical significance was determined using a one-way ANOVA with Tukey's post-hoc test ($^{*}p < 0.05$, $^{**}p < 0.01$).

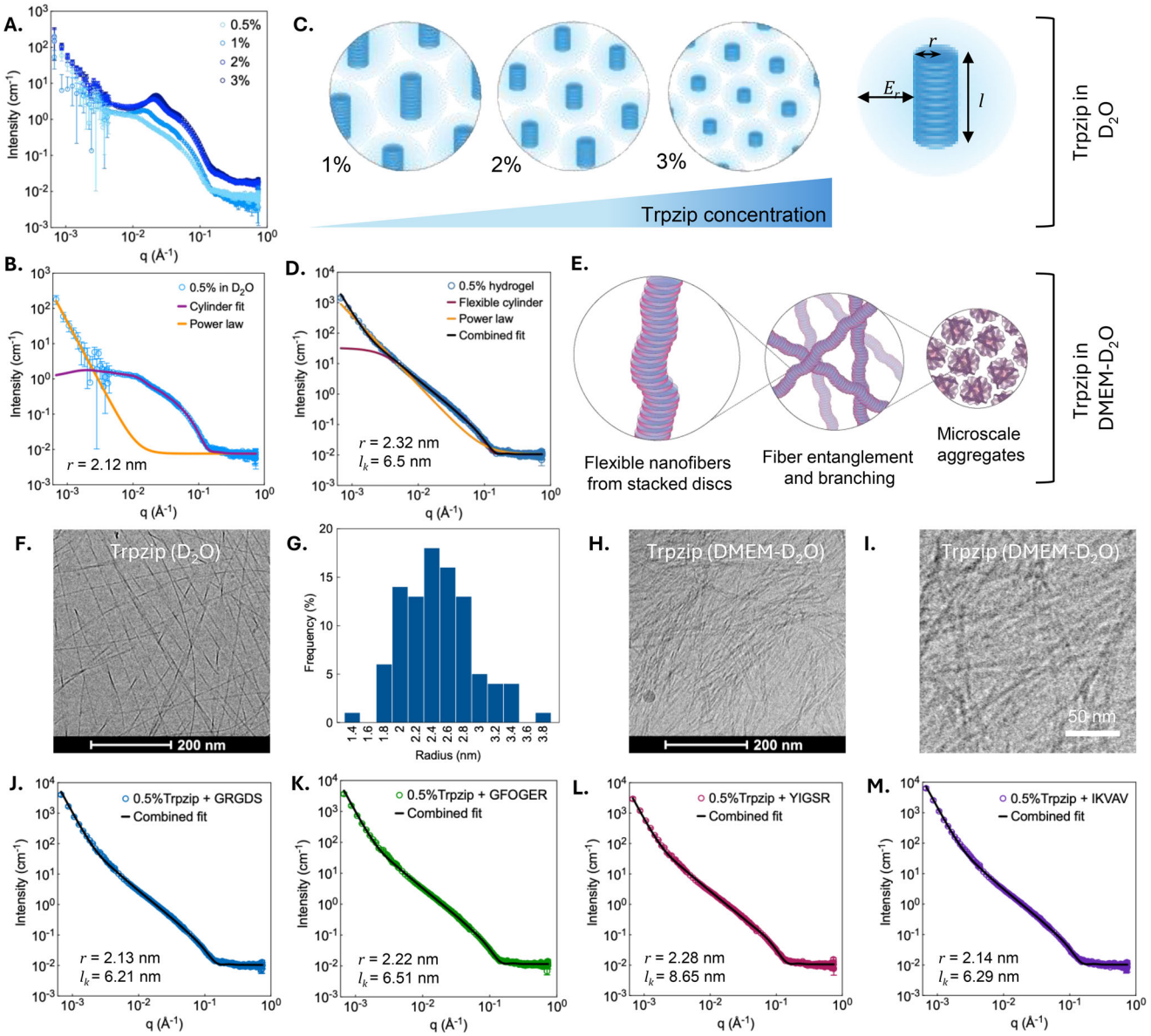

Figure 2. Small angle neutron scattering of Trpzip solutions and hydrogels. A) Scattering intensity profiles of Trpzip solutions in D_2O at varying concentrations. B) Representative fit of 0.5% Trpzip in D_2O using a combination of cylinder and power law models. C) Schematic of Trpzip self-assembly in D_2O based on SANS-derived trends showing decreased nanofiber radius, length, and effective interaction radius with increasing Trpzip concentration (values from Table S2, Supporting Information); not to scale. D) Scattering profile of a 0.5% Trpzip hydrogel in DMEM-D_2O, modeled with a flexible cylinder and power law fit. E) Schematic of hierarchical assembly and structure formation in Trpzip hydrogels prepared in DMEM-D_2O. F) CryoTEM image of Trpzip nanofibers in D_2O. G) Quantification of nanofiber radius of Trpzip peptides prepared in pure D_2O. H,I) CryoTEM image of Trpzip nanofibers in DMEM-D_2O. J–M) Scattering profiles of 0.5% Trpzip-ligand hydrogels (GRGDS, GFOGER, YIGSR, IKVAV) in DMEM-D_2O with combined flexible cylinder and power law model fits.

All concentrations exhibited a broad peak in the intermediate Q range corresponding to ordered interfibrillar spacing, with the peak's intensity increasing with peptide concentration.

To extract quantitative structural information, scattering profiles were fit using a combination of models: a Hayter–Penfold rescaled mean spherical approximation to account for electrostatic repulsion, a rigid cylinder model in the high-Q regime, and a power law in the low-Q regime (Figure 2B; Table S2 and Figure S11, Supporting Information). For more detailed explanations of the model fits used, refer to the Supporting Information Notes. As peptide concentration increased from 0.5% to 3%, the nanofiber radius (r) decreased from 2.26 ± 0.01 to 2.12 ± 0.002 nm, suggesting denser nanofiber packing at higher concentrations (Figure 2C). This compaction may be the result of a decrease in the number of peptides per lamellae or disc, as indicated by a reduction in effective particle charge from 7.17 ± 7.57 to 4.77 ± 0.24. Interestingly, nanofiber length (l) decreased significantly from 235.1 ± 14.4 to 99.7 ± 0.21 nm with

increasing concentration, and the effective interaction radius (E_r) was reduced from 23 ± 0.09 to 13 ± 0.24 nm, indicating weaker interfibril repulsion at higher concentrations. Additionally, increasing peptide concentration also led to a decrease in the Porod exponent from 2.94 ± 0.32 to 2.24 ± 0.17, indicating a structural transition in the Trpzip network from compact to more densely branched fractal networks. Together, these data indicate that Trpzip peptides in pure D_2O form short, rigid cylindrical nanofibers that organize into loosely connected mass fractals with decreasing compaction at higher peptide concentrations.

Upon gelation of the Trpzip solution induced by the addition of deuterated DMEM, the resulting hydrogel exhibited distinctly different scattering behavior to Trpzip peptides in pure D_2O. The best model fit for the gelled Trpzip network was a flexible cylinder model in the high-Q regime, rather than the rigid cylinder model used for peptide solutions (Figure 2D; Table S3 and Figure S11, Supporting Information). For more detailed explanations of the model fits used, refer to the Supplementary Notes. This change in model fits suggests that during gelation, the initially rigid and short nanofibers become more flexible and disordered, enabling the entanglement and hierarchical branching that ultimately form a Trpzip hydrogel (Figure 2E). The disappearance of the intermediate-Q peak also suggests a loss of long-range order in interfibrillar spacing. While the nanofiber radius remained relatively unchanged (2.24 ± 0.03 nm) between Trpzip nanofibers in the liquid versus gel state, the nanofiber length increased beyond the instrument's detection range (>1 μm), indicating extensive fiber elongation occurring during gelation. Additionally, the low-Q region suggested the formation of micro-scale aggregates with rough surface features, supported by a Porod exponent of 3.57 ± 0.039. Cryo-TEM imaging of Trpzip formulations further corroborated our SANS findings. Trpzip nanofibers (0.5% in D_2O) appeared as long, unbranched filaments with an average radius of 2.35 ± 0.17 nm (Figure 2F,G), closely matching the values obtained from SANS fitting. The presence of extended, continuous fibers likely reflects ongoing self-assembly during the overnight incubation prior to snap-freezing. When prepared in deuterated DMEM (0.5%), Trpzip nanofibers exhibited pronounced lateral bundling and reduced interfiber spacing (Figure 2H,I), consistent with enhanced ionic screening and reduced electrostatic repulsion in the culture medium. These observations visually confirm the transition from discrete nanofibers in D_2O to more compact, entangled aggregates in DMEM-D_2O, aligning with the proposed changes in nanofiber architecture from the SANS characterization. These structural changes are also consistent with rheological data comparing 0.5% Trpzip in water versus gelled 0.5% Trpzip in water/DMEM mixtures, with the rapid gelation of Trpzip in water reflecting the fast organization of rigid and well-ordered short nanofibers, while the slower DMEM-induced gelation reflects a more disordered self-assembly process resulting from the branched entanglement of longer nanofibers (Figure S2, Supporting Information). Altogether, the scattering profile of gelled Trpzip networks points to substantial structural reorganization during gelation, with longer and more flexible nanofibers forming branched, entangled networks with rough fractal microscale aggregation.

We next examined the effect of adhesive ligand incorporation on hydrogel nanostructure by performing SANS on Trpzip-ligand hydrogel formulations (200 μM). Similar to unmodified Trpzip hydrogels, all scattering profiles fit well with a combination of a flexible cylinder model in the high-Q region and a power law model in the low-Q region (Figure 2J–M; Table S3, Supporting Information). Fiber radii remained consistent across all Trpzip-ligand networks, ranging from 2.13 to 2.28 nm (all ± 0.02 nm), indicating that ligand incorporation does not disrupt core nanofiber dimensions, as also observed in cryoTEM imaging (Figure S4, Supporting Information). However, notable differences were observed in the Kuhn's length (l_k), which is a measure of nanofiber flexibility. Trpzip-GRGDS, Trpzip-GFOGER, and Trpzip-IKVAV hydrogels exhibited l_k values of 6.21, 6.51, and 6.29 nm (all ± 0.02 nm), respectively, showing similar nanofiber flexibility to that of unmodified Trpzip networks. However, Trpzip-YIGSR hydrogels showed a striking increase in Kuhn's length (8.65 ± 0.17 nm), suggesting a much more rigid nanofiber network despite unchanged fiber radius.

We then analyzed hydrogels composed entirely of Trpzip-ligand peptides (e.g., 100% ligand-functionalized sequences without unmodified Trpzip). These fully substituted matrices exhibited distinct nanostructure features compared to unmodified Trpzip hydrogels and mixed formulations (Figure S3A–D and Table S3, Supporting Information). Specifically, Trpzip-GFOGER and Trpzip-YIGSR formed highly rigid nanofibers (l_k = 9.1 and 14.4 nm, respectively) and exhibited high Porod exponents (>3), indicative of dense and well-ordered aggregates. In contrast, Trpzip-IKVAV hydrogels formed more flexible nanofibers (l_k = 4.02 nm) with a Porod exponent of 2.85, consistent with a more disordered and branched fractal network. Trpzip-GRGDS hydrogels also formed branched networks but with slightly more rigid nanofibers (l_k = 5.9 nm) and a lower Porod exponent of 2.7, pointing to moderately rigid fibers comprising a more loosely entangled network. Collectively, these SANS analyses demonstrate that small variations in sequence, concentration, and buffer conditions can significantly influence the nanostructure and hierarchical assembly of Trpzip-based hydrogels. This tunability allows for the design of either softer, entangled networks or stiffer and more ordered fibrillar scaffolds, providing a design roadmap for engineering mechanical and biochemical properties in synthetic Trpzip matrices.

Next, we investigated whether Trpzip hydrogels support the growth and maintenance of human iPSCs in the absence of adhesive ligands. To do so, we encapsulated dissociated iPSCs inside unmodified Trpzip matrices gelled with mTeSR, an iPSC-specific culture medium. Cells were seeded either as single cells or as small aggregates (20–100 μm diameter) in soft Trpzip hydrogels (~1 kPa stiffness) and cultured for 7 days (**Figure 3A**). By day 7, iPSCs embedded as single cells had merged into small spheroids, while aggregate-seeded iPSCs had expanded ~4 times in size into substantially larger spheroids (Figure S5A,B, Supporting Information). Furthermore, although iPSCs could survive dissociation and embedding in non-adhesive Trpzip matrices with no additional supplements, we found the addition of 10 μM ROCK inhibitor during the first 24 h post-dissociation markedly improved iPSC spheroid survival and growth (Figure 3A), as expected based on the known role of ROCK inhibitor as a preventor of programmed cell death via anoikis.

Leveraging the low-yield stress behavior of Trpzip hydrogels, spheroids were gently extracted from Trpzip matrices after 7 days in culture via user-applied shear force, which minimized

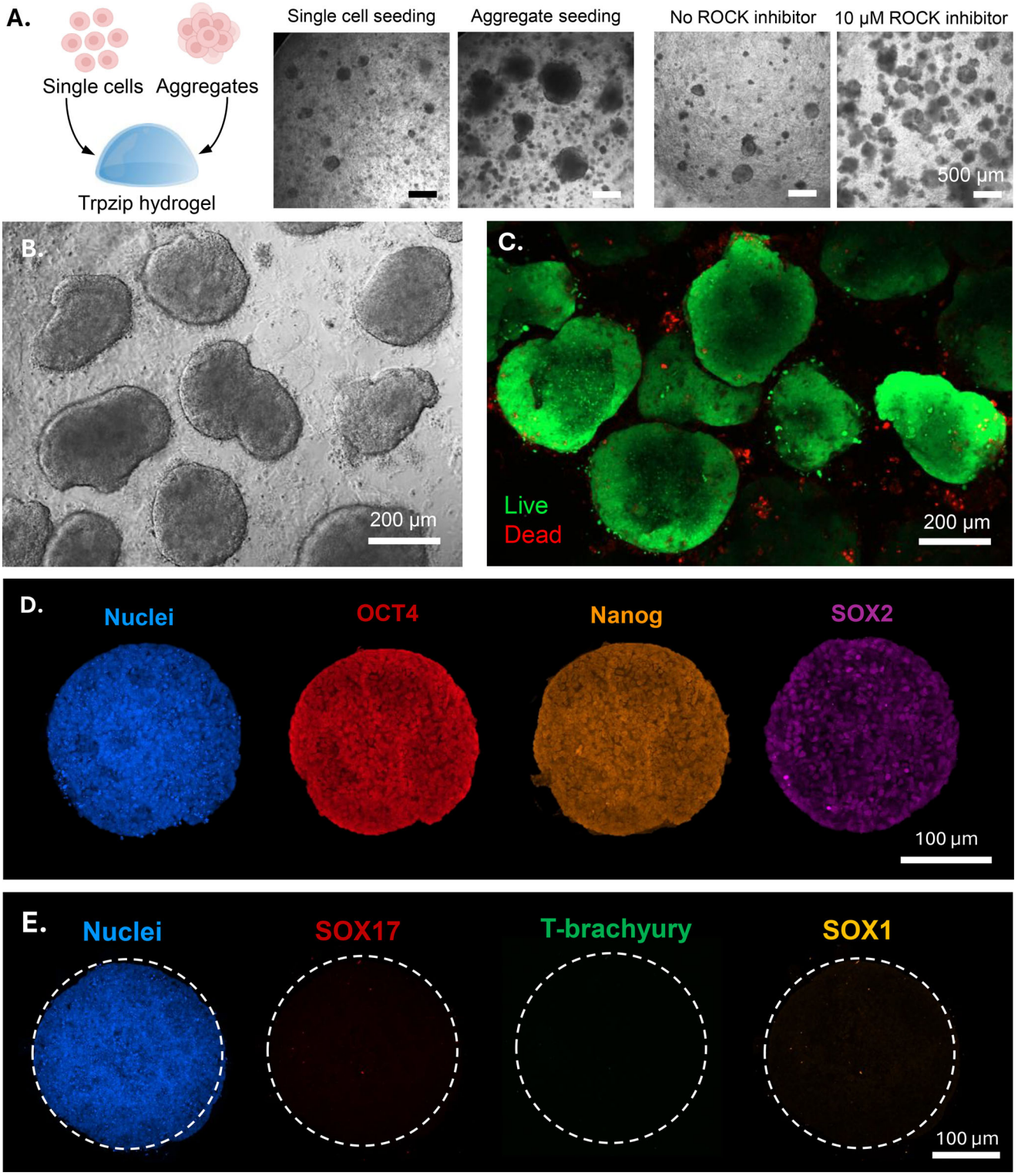

Figure 3. Growth of iPSCs embedded in Trpzip hydrogels without adhesive cues. A) Schematic and brightfield images comparing iPSC seeding strategies and the effect of ROCK inhibitor on iPSC growth and proliferation within Trpzip hydrogels. B) Brightfield image showing representative iPSC spheroids released from Trpzip hydrogels after seven days of culture. C) Live/Dead staining of encapsulated iPSC spheroids in Trpzip hydrogels showing live (green) and dead (red) cells. D) Immunofluorescence staining of iPSC spheroids for nuclei (blue) and the pluripotency markers OCT4 (red), Nanog (orange), and SOX2 (purple). E) Immunofluorescence staining of iPSC spheroids for nuclei(blue) and early germ layer markers SOX17 (endoderm, red), T-brachyury (mesoderm, green), and SOX1 (ectoderm, yellow).

mechanical damage or loss of cell viability in spheroids (Figure 3B). Live/Dead staining with Calcein AM and ethidium homodimer confirmed high cell viability within Day 7 spheroids, with little to no necrosis observed in the core of the spheroids (Figure 3C). To assess the ability of iPSCs to maintain pluripotency in Trpzip hydrogels, immunofluorescence staining was performed. The extracted spheroids were stained for key pluripotent transcription factors such as OCT4, Nanog, and SOX2 (Figure 3D). All markers showed strong and uniform nuclear localization, and the compact spheroid morphology was accompanied by strong cortical F-actin expression, highly akin to typical pluripotent architecture seen in embryoid bodies formed in suspension cultures (Figure S6A,B, Supporting Information). In contrast, immunostaining for early germ layer markers such SOX17 (endoderm), T-brachyury (mesoderm), and SOX1 (ectoderm) showed negligible expression in all spheroids (Figure 3E). These results demonstrate that Trpzip hydrogels, even in the absence of exogenous adhesive ligands, can provide a supportive 3D microenvironment that preserves iPSC viability, promotes proliferation, and maintains pluripotency without spontaneous differentiation.

Since adhesion motifs are known to exert an influence on stem cell decision making, we next evaluated whether Trpzip alone or the Trpzip-ligand hydrogels might bias iPSC differentiation toward specific germ layer lineages. To do so, we encapsulated iPSC aggregates in Trpzip matrices functionalized with 200 μM GRGDS, GFOGER, YIGSR, or IKVAV, alongside unmodified Trpzip as a control (**Figure 4A**). While Matrigel is a widely used ECM matrix, it was not suitable as a control in this study. In preliminary trials, iPSCs encapsulated in Matrigel dispersed throughout the gel rather than forming stable spheroids, presumably due to the high content of ECM proteins, some of which can facilitate migration.[19] Following encapsulation, spheroids were allowed to stabilize for 7 days in mTeSR media prior to the induction of each germ layer specification using defined differentiation media targeting endoderm, mesoderm, or ectoderm outcomes (Figure 4B). Over the 12-day differentiation timeline, a four to fivefold increase in spheroid size was observed across all lineages, regardless of ligand presentation in Trpzip hydrogels (Figure 4C), suggesting that overall cell proliferation was not significantly impacted by the presence or absence of specific adhesive cues. No appreciable degradation was observed during the 12-day culture period, although future work will explore long-term hydrogel stability and cell-mediated remodeling in the context of extended tissue culture and organoid development.

To assess whether ligand presentation influenced iPSC lineage commitment, we performed immunofluorescence staining of early germ layer markers on the differentiated spheroids. For endodermal differentiation, spheroids were stained for the early endoderm marker SOX17 and the definitive endoderm marker FOXA2 (Figure 4D; Figure S7, Supporting Information). Surprisingly, unmodified Trpzip hydrogels (lacking any adhesive ligand) supported the highest expression of both transcription factors, followed by Trpzip-GRGDS matrices (Figure 4E). Spheroids in Trpzip-GFOGER hydrogels exhibited the lowest levels of endodermal expression. Mesodermal spheroids were assessed for the early mesoderm marker T-brachyury, the cell adhesion molecule N-cadherin, and Collagen IV, a basement membrane protein that plays a crucial role in mesodermal development (Figure 4F; Figure S8, Supporting Information). Amongst all matrices, Trpzip-GRGDS hydrogels most robustly promoted mesodermal differentiation, showing a threefold increase in T-brachyury expression compared to unmodified Trpzip, as well as significantly higher expression of N-cadherin and Collagen IV (Figure 4G; Figures S8 and S9, Supporting Information). Spheroids grown in Trpzip-GFOGER matrices also showed enhanced T-brachyury expression relative to unmodified Trpzip spheroids, albeit to a lesser extent. In contrast, YIGSR- and IKVAV-functionalized hydrogels showed the lowest support of mesodermal differentiation. For ectodermal differentiation, spheroids were stained for the early ectoderm marker SOX1 and the neuroectoderm marker PAX6 (Figure 4H; Figure S10, Supporting Information). Trpzip-IKVAV matrices showed the strongest induction of both ectodermal markers, with a threefold increase in SOX1 and a 2.5-fold increase in PAX6 expression intensity relative to unmodified Trpzip hydrogels (Figure 4I). Interestingly, Trpzip-YIGSR matrices enhanced early SOX1 expression but were less effective at upregulating PAX6, suggesting sufficient support for early ectoderm but not further neural commitment. In contrast, GRGDS matrices showed twice the expression of both SOX1 and PAX6 relative to the control, suggesting consistent support of neuroectoderm fate. GFOGER-functionalized and Trpzip-only hydrogels showed the lowest support for ectodermal differentiation. In sum, it was found that unmodified Trpzip matrices with no ligands present best support endodermal differentiation, the presence of GRGDS enhances mesodermal commitment, and IKVAV- and YIGSR-functionalized matrices promote ectodermal development. Of note, Trpzip-GFOGER hydrogels did not appear to improve the differentiation outcomes for any of the three germ layers compared to other Trpzip-ligand hydrogels. Together, these findings demonstrate that Trpzip hydrogels presenting different adhesive cues can influence iPSC lineage commitment in a ligand-specific manner.

Comparison of the macroscale properties (hydrogel stiffness and mechanical strength) and nanoscale properties (nanofiber dimension and rigidity) of the various Trpzip-ligand matrices revealed distinct correlations with lineage outcomes (**Figure 5**). Unmodified Trpzip hydrogels, which exhibited intermediate stiffness and mechanical strength, combined with slightly more flexible nanofibers, provided the strongest support of endodermal differentiation. This finding aligns with previous studies suggesting that integrin activation can suppress endodermal specification by activating the Akt signaling pathway through integrin-linked kinase (ILK).[20] In addition, successful endodermal differentiation has been achieved in xeno-free hydrogels like alginate,[21] which lack integrin-binding motifs altogether, reinforcing the notion that integrin-free microenvironments are permissive for endoderm development. While the observed trends in SOX17 and FOXA2 expression reflect the relative endodermal potential of each matrix at the chosen endpoint, it is possible that other matrix ligands more robustly promote endoderm fate before or after this narrow window. Future studies incorporating time-course RT-qPCR will be valuable for resolving these temporal dynamics and further elucidating how Trpzip matrix composition influences differentiation trajectories.

For mesodermal differentiation, Trpzip-GRGDS matrices markedly enhanced expression of mesodermal markers compared to all other ligand-functionalized hydrogels.

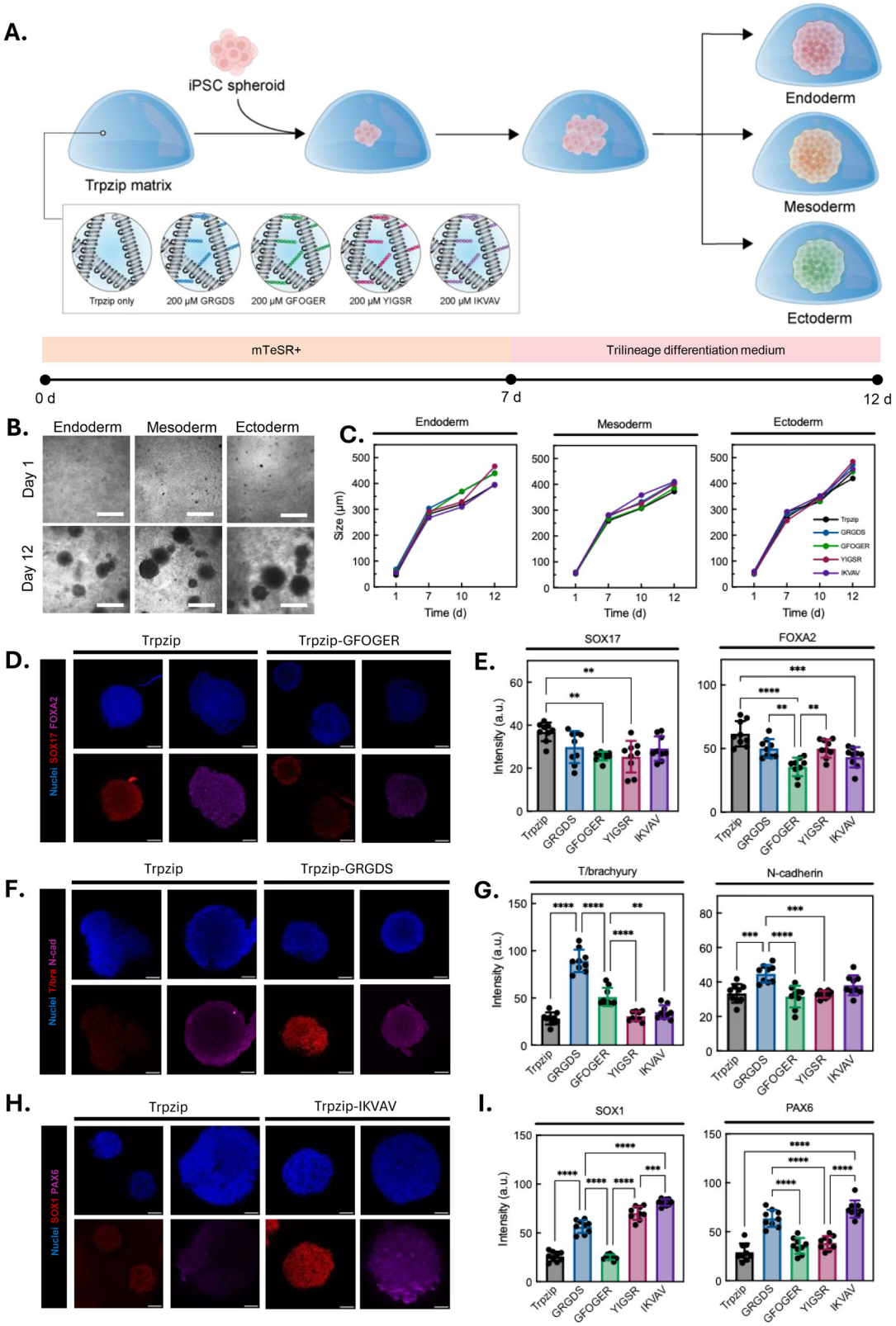

Figure 4. Trilineage differentiation of iPSCs in Trpzip hydrogels. A) Schematic detailing experimental timeline for iPSC spheroid culture and differentiation in Trpzip-ligand hydrogels. B) Brightfield images of iPSC spheroids undergoing directed differentiation toward endoderm, mesoderm, and ectoderm fates at day 1 and day 12. Scale is 500 μm. C) Quantification of spheroid size during lineage-specific differentiation in Trpzip hydrogels functionalized with different adhesive ligands. D) Representative immunofluorescence staining of endodermal markers SOX17 (red) and FOXA2 (purple) in spheroids

cultured in non-functionalized Trpzip and GFOGER-functionalized Trpzip hydrogels. E) Quantification of SOX17 and FOXA2 staining intensities across Trpzip-ligand hydrogel matrices. Data is shown as mean ± s.d. from n £ 9 spheroids. Statistical significance was determined using a one-way ANOVA with Tukey's post-hoc test ($^{*}p < 0.05$, $^{**}p < 0.01$, $^{***}p < 0.001$, $^{****}p < 0.0001$). F) Representative immunofluorescence staining of mesodermal markers T-brachyury (red) and N-cadherin (purple) in non-functionalized Trpzip and GRGDS-functionalized Trpzip hydrogels. G) Quantification of T-brachyury and N-cadherin staining intensities across Trpzip-ligand hydrogel matrices. Data is shown as mean ± s.d. from n = 9 spheroids. Statistical significance was determined using a one-way ANOVA with Tukey's post-hoc test ($^{*}p < 0.05$, $^{**}p < 0.01$, $^{***}p < 0.001$, $^{****}p < 0.0001$). H) Representative immunofluorescence staining of ectodermal markers SOX1 (red) and PAX6 (purple) in non-functionalized Trpzip and IKVAV-functionalized Trpzip hydrogels. Nuclei are stained in blue (DAPI) in all panels. Scale is 100 µm. I) Quantification of SOX1 and PAX6 staining intensities across Trpzip-ligand hydrogel matrices. Data is shown as mean ± s.d. from n = 9 spheroids. Statistical significance was determined using a one-way ANOVA with Tukey's post-hoc test ($^{*}p < 0.05$, $^{**}p < 0.01$, $^{***}p < 0.001$-, $^{****}p < 0.0001$).

Trpzip-GRGDS hydrogels possessed similar mechanics and nanofiber characteristics to other ligand formulations, suggesting the presence of the GRGDS motif itself was the main driver behind improved mesodermal commitment. This is supported by studies showing that fibronectin, from which the GRGDS motif is derived, plays a dominant role in promoting mesodermal and endothelial differentiation in both 3D in vitro and in vivo systems.[22] Interestingly, collagen matrices alone were not effective at enhancing mesodermal development, an observation that aligns with our findings. We similarly observed that Trpzip-GFOGER hydrogels failed to promote mesoderm differentiation as robustly as Trpzip-GRGDS matrices. In another study, the loss of fibronectin-derived RGD motifs dramatically impaired mesoderm development in both pluripotent mouse cells and zebrafish embryos.[23] These studies highlight that engagement of integrin-β1 by GRGDS is critical for activating signaling cascades that drive mesodermal fates. Conversely, loss of collagen-derived GFOGER cues in the same models had little impact on mesoderm differentiation efficiency, further supporting the notion that RGD-mediated signaling plays a more dominant role in mesodermal lineage commitment.

Finally, we observed that ectodermal fate was most enhanced in Trpzip-IKVAV hydrogels. Other studies have similarly shown that the IKVAV motif promotes neural differentiation of iPSCs and neural progenitors in both 2D and 3D systems,[24] outperforming other laminin- or fibronectin- derived motifs such as YIGSR and RGD. Another recent study investigating human iPSC-derived neural differentiation on 2D peptide nanofibers functionalized with IKVAV found that increased "molecular motion" of the peptide nanofibers played a key role in neural differentiation and maturation,[25] highlighting how both IKVAV-based adhesion and dynamic nanostructure properties can work complementarily in directing ectodermal outcomes. Across all Trpzip-ligand conditions, Trpzip-IKVAV hydrogels possessed higher stiffness and mechanical strength alongside higher fiber flexibility at the nanoscale. These combined properties of Trpzip-IKVAV hydrogels with stiffer bulk mechanics coupled with more local matrix flexibility may mimic the mechanical landscape of the developing neuroepithelium and account for the improved ectodermal and neural commitment observed.

There are a limited number of other studies that have interrogated how ligand identity in fully synthetic 3D hydrogels influences germ layer specification of iPSCs. Many prior trilineage differentiation studies in 3D engineered hydrogels have relied on generic adhesive motifs such as RGD[26] or incorporated natural proteins such as gelatin[27] to broadly support adhesion without tailoring toward specific lineages. Some studies incorporate alternate ECM-derived peptides, such as YIGSR and IKVAV, but typically in the context of enhancing one target cell fate, such as promoting lung[28] or neural progenitors.[29] Recent work utilizing 3D peptide hydrogels in iPSC trilineage studies have focused only on the role of soluble cues such as BMP4[30] or embryoid induction cocktails[31] in the absence of any adhesive ligands. Our findings add to ongoing efforts to define how adhesive ligand

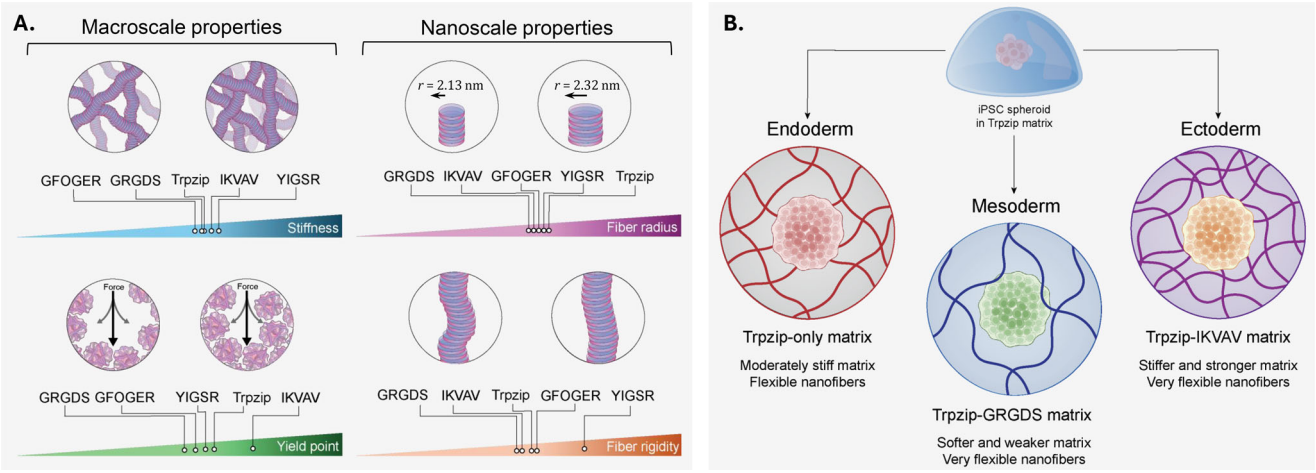

Figure 5. Conceptual summary of Trpzip-ligand hydrogels nanoscale and macroscale materials characterization and support of the three germ layer commitments in differentiating iPSCs. A) Schematic displaying the overall differences in macroscale properties such as hydrogel stiffness and mechanical strength (yield point) and nanoscale properties such as nanofiber radius and rigidity. B) Trpzip-ligand hydrogel that best supported the lineage commitment of differentiating iPSCs to endoderm, mesoderm, and ectoderm fates.

presentation contributes to iPSC fate specification, particularly within synthetic 3D microenvironments. Such approaches will be increasingly useful for refining how matrix composition can be engineered to direct stem cell fate in reproducible, modular, and xeno-free 3D culture systems.

Taken together, these results highlight that the biological outcome of a synthetic niche is not dictated solely by individual material parameters but rather by the combined presentation of mechanical properties, nanostructure, and biochemical ligands. While the Kuhn length and Porod exponent derived from the SANS fittings provide ensemble-averaged estimates of nanofiber rigidity, these parameters do not resolve molecular-scale flexibility. Figure 5 should be interpreted as a conceptual summary of experimentally observed trends rather than a molecular-level model. Future studies employing complementary techniques such as SAXS, molecular dynamics simulations, or dark-field microscopy for persistence length analysis are warranted to probe Trpzip nanofiber flexibility at higher structural resolution. Future work, such as combinatorial ECM motif incorporation in precise ratios using ligand blends could further improve the capability of Trpzip hydrogels to mimic developmental microenvironments and guide stem cell fate. In addition, integrating or layering Trpzip variants presenting distinct adhesive motifs may provide a way to spatially guide coordinated germ-layer patterning, potentially enabling synthetic models of early tissue organization and biofabricated constructs with hierarchical structure.

3. Conclusion

In this study, we developed a modular peptide hydrogel platform based on the self-assembling Trpzip motif, engineered to present a range of adhesive ligands derived from key ECM proteins (fibronectin, collagen, and laminin). Through SANS and rheological analyses, we demonstrate that integration of these adhesion sequences only slightly modulates peptide network architecture and bulk hydrogel mechanics. However, while Trpzip-ligand hydrogels maintain similar nanofiber dimensions and matrix stiffness, it was found that incorporation of adhesive motifs can subtly alter nanofiber flexibility and supramolecular organization. Of the different Trpzip-ligand hydrogels assessed, we found endodermal commitment is enhanced by Trpzip matrices of intermediate stiffness without integrin ligands, mesodermal fate is promoted in softer matrices with flexible, GRGDS-bearing nanofibers, and ectodermal lineages are best supported by stiffer yet still flexible nanofibers presenting neural-promoting motifs such as IKVAV and YIGSR. These findings establish a design framework in which specific combinations of bulk hydrogel mechanics, nanofiber flexibility, and adhesive motifs can be selected to steer iPSC fate toward desired lineages in a fully synthetic 3D matrix.

As the demand for chemically defined and xeno-free biomaterials in biofabrication continues to grow, this work demonstrates the potential of Trpzip-based peptide materials to fulfill this need by coupling the advantages of fully synthetic hydrogels with the biological functionality of native ECMs. By providing a well-defined, fully synthetic matrix with modular biochemical adhesion cues, this work establishes Trpzip hydrogels as a versatile platform for engineering 3D stem cell niches and directing specific differentiation outcomes. Their simplicity, scalability, and unique mechanical properties position them as promising biomaterials for biofabrication with translational applications ranging from developmental modeling, therapeutic cell manufacturing, and 3D tissue biofabrication.

4. Experimental Section

Materials: Synthetic peptides (Trpzip, Trpzip-GRGDS, Trpzip-GFOGER, Trpzip-YIGSR, and Trpzip-IKVAV) were purchased as the formate salt (purity >98%) from GenScript Biotech (Singapore) Pte Ltd and used without further purification. All peptide sequences are listed in Table S1 (Supporting Information) and are as follows: Trpzip (SWTWQGNVWTWK; 1578.75 g mol^{-1}), Trpzip-GRGDS (SWTWQGNVWTWKGRGDS; 2051.21 g mol^{-1}), Trpzip-GFOGER (SWTWQGNVWTWKGFOGER; 2125.33 g mol^{-1}), Trpzip-YIGSR (SWTWQGNVWTWKYIGSR; 2155.4 g mol^{-1}), and Trpzip-IKVAV (SWTWQGNVWTWKIKVAV; 2089.43 g mol^{-1}).

Hydrogel Fabrication: Trpzip hydrogels were prepared by dissolving lyophilized peptide in Milli-Q water at a concentration of 1% (w/v). Magnetic stirring on a hot plate (40 °C) was used to accelerate dissolution. Gelation was triggered by adding cell culture media to a final concentration of 0.5% (w/v). Trpzip-ligand hydrogels were prepared using peptide variants Trpzip-GRGDS, Trpzip-GFOGER, Trpzip-YIGSR, Trpzip-IKVAV. To prepare Trpzip-ligand hydrogels comprising 200 µM concentration of a ligand-containing peptide, peptides were dissolved in Milli-Q water (5 mM stock). Magnetic stirring on a hot plate (40 °C) was used to accelerate dissolution. Trpzip-ligand solution (400 µM) was added to pure Trpzip stock solution (1% w/v) and mixed thoroughly. Gelation was then triggered as usual, by adding cell culture media to achieve a final concentration of 0.5% (w/v) solid content, and 200 µM concentration of Trpzip-ligand. For Trpzip-ligand hydrogels composed entirely of Trpzip-ligand peptides, 1% (w/v) stock solutions were prepared using only the Trpzip-ligand peptides. Gelation was induced as above by adding cell culture media to achieve a final concentration of 0.5% (w/v).

Oscillatory Shear Rheology: Rheological measurements were performed on an Anton Paar MCR 302e Rheometer equipped with a parallel plate geometry (25 mm disc, 1 mm gap height, 560 µL of hydrogel). Oscillatory measurements were performed with 0.2% strain and 1 Hz frequency at 37 °C, unless specified otherwise. Strain sweep tests were performed immediately following 15 h time sweeps with a log ramp up rate from 0.2% shear strain up to 200% at 1 Hz frequency over 10 min. In all rheological tests, a humidity chamber with a reservoir of water was used to prevent drying of the peptide hydrogel.

Small Angle Neutron Scattering (SANS): Trpzip gels were prepared by dissolving lyophilized peptide in deuterated DMEM before being transported to Australian Centre for Neutron Scattering (ACNS) at the Australian Nuclear Science and Technology Organization (ANSTO). Deuterated DMEM was prepared by lyophilizing high-glucose DMEM and reconstituting the remaining solid in an equivalent volume of deuterium oxide (D_2O). SANS measurements were performed on hydrogels samples at 37 °C. The structure of the hydrogels was analyzed using the Quokka pinhole small-angle neutron scattering instrument.[32] Samples were loaded into 20 mm demountable cells with a 1 mm pathlength. Scattering data of samples were collected across a full q range of 0.0007–0.73 $Å^{-1}$ with three detector configurations (20 m collimation with 8.1 Å neutrons), 12 m (12 m collimation with 5 Å neutrons) and 1.3 m (12 m collimation with 5 Å neutrons). The scattering profiles of the gels were recorded against the scattering vector by using the following equation:

$$q = \frac{4\pi}{\lambda} sin\theta \quad (1)$$

where q is the scattering vector, 2θ is the angle of scattering, λ is the wavelength of the neutron beam. The obtained 2D raw scattering data were reduced and converted to the absolute scale using the Igor Pro software package[33] and Quokka SANS reduction macros. Igor Pro was used to

subtract appropriate solvent background from each dataset. SasView was used to fit the models to the scattering data.

Cryogenic TEM: Hydrogel (4 µL) was applied to glow discharged copper grids (Quantifoil R2/2, Quantifoil Micro Tools) and blotted for 4.5 s in a 100% humidity chamber at 4 °C, with a blotting force of 0. The grids were then plunge-frozen in liquid ethane using a Vitrobot Mark IV device (Thermo Fisher Scientific). The grids were imaged using a Talos Arctica cryoTEM (Thermo Fisher Scientific), operating at 200 kV with the specimen held at liquid nitrogen temperatures. Images were captured using a Falcon 3EC direct detector camera in linear mode.

Human iPSC Culture: Human iPSCs (ATCC, ACS-1020) were authenticated by ATCC using STR profiling and karyotyping, as confirmed by the Certificate of Analysis provided upon purchase. Pluripotency was also authenticated via immunofluorescence staining of pluripotency markers OCT4, SOX2, and Nanog prior to differentiation. iPSCs were cultured on plastic substrates coated with hESC-qualified Matrigel (Corning, #354277) diluted in DMEM/F12 media (STEMCELL Technologies, #36254) according to manufacturer's instructions. Media changes consisting of mTeSR Plus (STEMCELL Technologies, #100-0276) occurred every 24 h, except for one 48 h exchange once per week. iPSCs were passaged once they reached 70–80% confluency, approximately every 5–6 d. Cells were passaged using ReLeSR (STEMCELL Technologies, #100-0483) to selectively detach pluripotent colonies and mechanically fragmented into 50–100 µm aggregates before being reseeded at a density of 500 colonies mL^{-1}. All cultures were maintained at 37 °C and 5% CO_2. iPSCs were used between passages 19–29 for all experiments.

iPSC Encapsulation in Trpzip Hydrogels: For single cell dissociation, iPSCs were incubated with StemPro Accutase Cell Dissociation Reagent (Gibco, #A1110501) using a volume of 1 mL per 35-mm dish at 37 °C for 7 min. To ensure a single cell suspension, the harvested iPSCs were mechanically fragmented using a P1000 pipette until a single cell suspension was obtained. To collect iPSCs as small aggregates (~50–100 µm), iPSCs were incubated with ReLeSR using a volume of 1 mL per 35-mm dish for 10 s at RT, followed by aspiration of ReLeSR and an additional incubation for 3 min at 37 °C. Detached iPSC colonies were collected in mTeSR media and fragmented into appropriately sized aggregates using a 5 mL serological pipette. Cells were resuspended in 1 mL mTeSR medium supplemented with 10 µM ROCK inhibitor (STEMCELL technologies, #72304) and counted manually using a hemocytometer. Either single iPSCs or iPSC aggregates were mixed with Trpzip hydrogels (100 µL per 96-well) at a density of ~10–15 aggregates per gel. Trpzip gels with iPSCs were allowed to stiffen at 37 °C for 1 h before mTeSR medium supplemented with 10 µM ROCK inhibitor was gently overlaid on top of the gel surface. All media changes with mTeSR Plus following seeding occurred daily without ROCK inhibitor. All cultures were maintained at 37 °C and 5% CO_2.

Cell Viability Staining: For live/dead staining, Calcein-AM (0.5 µL mL^{-1}) and Ethidium–Homodimer-1 (2 µL mL^{-1}) from the LIVE/DEAD Viability/Cytotoxicity Kit for mammalian cells (Invitrogen, #L3224) were added to cell-laden Trpzip gels for 40 min at 37 °C before being washed twice with PBS prior to imaging.

Trilineage Differentiation: iPSC spheroids seeded in Trpzip hydrogels were cultured in mTeSR medium, with daily media changes for 7 d prior to initiating trilineage differentiations. Differentiation was achieved using the STEMdiff Trilineage Differentiation Kit (STEMCELL Technologies, #05230), prepared according to manufacturer's instructions.

Immunofluorescence Staining: Cells in Trpzip gels were fixed in 4% methanol-free PFA for 45 min at RT. Excess PFA was removed, and gels were washed three times in PBS. Samples were then permeabilized with 0.1% (v/v) tween-20 in PBS (10 min at RT). Blocking was performed using a blocking buffer (1% bovine serum albumin and 0.1% triton X-100 in PBS) for 20 min at RT. Primary antibodies were diluted in blocking buffer to their working concentration and incubated with fixed hydrogel samples overnight at 4 °C. Fixed samples were then washed in blocking buffer at least three times over the span of 1d before secondary antibodies were diluted in blocking buffer to their working concentration and incubated overnight at 4 °C. Fixed samples were then washed in blocking buffer at least three times over the span of 1 d before confocal imaging.

Confocal Microscopy: All immunofluorescence samples were imaged in 96-well glass bottom plates fitted with high-performance #1.5 cover glass using a Zeiss LSM 800 confocal microscope and Zen Blue software.

Statistical Analysis: GraphPad Prism (version 10.5.0) was used for statistical analysis of all data. Storage and loss moduli for strain sweep curves were normalized using min-max normalization. Data is presented as mean ± SD, with n = 3 sample size unless otherwise stated. Statistical significance was calculated using an ordinary one-way ANOVA with Tukey's multiple comparisons post-hoc test. Differences were considered significant when $p < 0.05$.

Supporting Information

Supporting Information is available from the Wiley Online Library or from the author.

Acknowledgements

This work was supported through funding from the UNSW Division of Research and Enterprise 3R Program, the Australian Research Council Grant DP230101804 (K.A.K.), and the National Cancer Institute of the National Institutes of Health Grant R01CA251443 (K.A.K.). The authors acknowledge the help and support of staff at the Katharina Gaus Light Imaging Facility (KGLMF) of the UNSW Mark Wainwright Analytical Centre.

Conflict of Interest

The authors declare no conflict of interest.

Data Availability Statement

The data that support the findings of this study are available from the corresponding author upon reasonable request.;

Keywords

differentiation, hydrogel, peptide, self-assembly, stem cell, iPSC

Received: July 21, 2025
Revised: October 27, 2025
Published online: November 7, 2025

[1] S. R. Braam, L. Zeinstra, S. Litjens, D. Ward-van Oostwaard, S. van den Brink, L. van Laake, F. Lebrin, P. Kats, R. Hochstenbach, R. Passier, A. Sonnenberg, C. L. Mummery, *STEM CELLS* **2008**, *26*, 2257.
[2] A. J. Engler, S. Sen, H. L. Sweeney, D. E. Discher, *Cell* **2006**, *126*, 677.
[3] S. Vukicevic, H. K. Kleinman, F. P. Luyten, A. B. Roberts, N. S. Roche, A. H. Reddi, *Exp. Cell Res.* **1992**, *202*, 1.
[4] H. K. Kleinman, M. L. McGarvey, J. R. Hassell, V. L. Star, F. B. Cannon, G. W. Laurie, G. R. Martin, *Biochemistry* **1986**, *25*, 312.
[5] C. S. Hughes, L. M. Postovit, G. A. Lajoie, *Proteomics* **2010**, *10*, 1886.
[6] N. C. Talbot, T. J. Caperna, *Cytotechnology* **2015**, *67*, 873.
[7] J. Li, X. Du, D. J. Powell, R. Zhou, J. Shi, H. He, Z. Feng, B. Xu, *Chem. Asian J.* **2018**, *13*, 3464.
[8] K. S. Hellmund, B. Koksch, *Front. Chem.* **2019**, *7*, 172.
[9] C. Diaferia, M. Ghosh, T. Sibillano, E. Gallo, M. Stornaiuolo, C. Giannini, G. Morelli, L. Adler-Abramovich, A. Accardo, *Soft Matter* **2019**, *15*, 487.

[10] M. Goktas, G. Cinar, I. Orujalipoor, S. Ide, A. B. Tekinay, M. O. Guler, *Biomacromolecules* **2015**, *16*, 1247.
[11] Y. Ding, Y. Li, M. Qin, Y. Cao, W. Wang, *Langmuir ACS J. Surf. Colloids* **2013**, *29*, 13299.
[12] G. Fichman, J. P. Schneider, *Front. Bioeng. Biotechnol.* **2020**, *8*, 594258.
[13] M. Vitale, C. Ligorio, I. P. Smith, S. M. Richardson, J. A. Hoyland, J. Bella, *Gels Basel Switz.* **2022**, *8*, 254 .
[14] A. K. Nguyen, T. G. Molley, E. Kardia, S. Ganda, S. Chakraborty, S. L. Wong, J. Ruan, B. E. Yee, J. Mata, A. Vijayan, N. Kumar, R. D. Tilley, S. A. Waters, K. A. Kilian, *Nat. Commun.* **2023**, *14*, 6604.
[15] M. D. Pierschbacher, E. Ruoslahti, *Nature* **1984**, *309*, 30.
[16] C. G. Knight, L. F. Morton, A. R. Peachey, D. S. Tuckwell, R. W. Farndale, M. J. Barnes, *J. Biol. Chem.* **2000**, *275*, 35.
[17] J. Graf, R. C. Ogle, F. A. Robey, M. Sasaki, G. R. Martin, Y. Yamada, H. K. Kleinman, *Biochemistry* **1987**, *26*, 6896.
[18] K. Tashiro, G. C. Sephel, B. Weeks, M. Sasaki, G. R. Martin, H. K. Kleinman, Y. Yamada, *J. Biol. Chem.* **1989**, *264*, 16174.
[19] G. Benton, I. Arnaoutova, J. George, H. K. Kleinman, J. M. Koblinski, *Adv. Drug Delivery Rev.* **2014**, *79–80*, 3.
[20] P. J. Wrighton, J. R. Klim, B. A. Hernandez, C. H. Koonce, T. J. Kamp, L. L. Kiessling, *Proc. Natl. Acad. Sci., U. S. A.* **2014**, *111*, 18126.
[21] M. M. Capeling, M. Czerwinski, S. Huang, Y.-H. Tsai, A. Wu, M. S. Nagy, B. Juliar, N. Sundaram, Y. Song, W. M. Han, S. Takayama, E. Alsberg, A. J. Garcia, M. Helmrath, A. J. Putnam, J. R. Spence, *Stem Cell Rep.* **2019**, *12*, 381.
[22] S. Battista, D. Guarnieri, C. Borselli, S. Zeppetelli, A. Borzacchiello, L. Mayol, D. Gerbasio, D. R. Keene, L. Ambrosio, P. A. Netti, *Biomaterials* **2005**, *26*, 6194.
[23] P. Cheng, P. Andersen, D. Hassel, B. L. Kaynak, P. Limphong, L. Juergensen, C. Kwon, D. Srivastava, *Dev. Camb. Engl.* **2013**, *140*, 2587.
[24] J. Lam, S. T. Carmichael, W. E. Lowry, T. Segura, *Adv. Healthcare Mater.* **2015**, *4*, 534.
[25] Z. Álvarez, J. A. Ortega, K. Sato, I. R. Sasselli, A. N. Kolberg-Edelbrock, R. Qiu, K. A. Marshall, T. P. Nguyen, C. S. Smith, K. A. Quinlan, V. Papakis, Z. Syrgiannis, N. A. Sather, C. Musumeci, E. Engel, S. I. Stupp, E. Kiskinis, *Cell Stem Cell* **2023**, *30*, 219-238.e14.
[26] L. Wang, L. Riediger, Q. Rao, X. Xu, Y. Nie, Y. Zhou, J. Zhang, P. Tang, W. Wang, F. Tacke, A. Guillot, L. Vallier, I. Talon, W. Li, Y.-A. Yang, R. Haag, N. Ma, *Adv. Funct. Mater.* **2025**, 08430.
[27] M. R. Arkenberg, Y. Ueda, E. Hashino, C.-C. Lin, *Stem Cell Res. Ther.* **2023**, *14*, 223.
[28] A. E. Tanneberger, R. Blomberg, G. Bilousova, A. L. Ryan, C. M. Magin, *Am. J. Physiol.-Lung Cell. Mol. Physiol.* **2025**, *328*, L379.
[29] E. M. Ovadia, D. W. Colby, A. M. Kloxin, *Biomater. Sci.* **2018**, *6*, 1358.
[30] H. S. Alsehli, E. Roy, T. Williams, A. Kuziola, Y. Guo, C. A. Dreiss, J. B. A. Green, E. Gentleman, D. Danovi, *Front. Bioeng. Biotechnol.* **2024**, *12*, 1467412.
[31] M. S. Rahman, G. Qi, Q. Li, X. Liu, J. Bai, M. Chen, A. Atala, X. S. Sun, *Bioengineering* **2025**, *12*, 503.
[32] K. Wood, J. P. Mata, C. J. Garvey, C.-M. Wu, W. A. Hamilton, P. Abbeywick, D. Bartlett, F. Bartsch, P. Baxter, N. Booth, W. Brown, J. Christoforidis, D. Clowes, T. d'Adam, F. Darmann, M. Deura, S. Harrison, N. Hauser, G. Horton, D. Federici, F. Franceschini, P. Hanson, E. Imamovic, P. Imperia, M. Jones, S. Kennedy, S. Kim, T. Lam, W. T. Lee, M. Lesha, et al., *J. Appl. Crystallogr.* **2018**, *51*, 294.
[33] S. R. Kline, *J. Appl. Crystallogr.* **2006**, *39*, 895.